Communication

High Performance Nanostructured Supercapacitors on a Sponge

Husam Niman Alshareef, Wei Chen, R B Rakhi, Liangbing Hu, Xing Xie, and Yi Cui

Nano Lett., **Just Accepted Manuscript** • Publication Date (Web): 16 September 2011

High Performance Nanostructured Supercapacitors on a Sponge

Wei Chen[1], R. B. Rakhi[1], Liangbing Hu[2], Xing Xie[3], Yi Cui [2], H. N. Alshareef[,1]*

1 Materials Science and Engineering, King Abdullah University of Science and Technology (KAUST), Jeddah, Saudi Arabia 23955-6900; 2 Department of Materials Science and Engineering, Stanford University, California, USA 94305; 3 Department of Civil and Environmental Engineering, Stanford University, Stanford, California, USA 94305

*To whom correspondence should be addressed, E-mail: husam.alshareef@kaust.edu.sa

TABLE OF CONTENTS

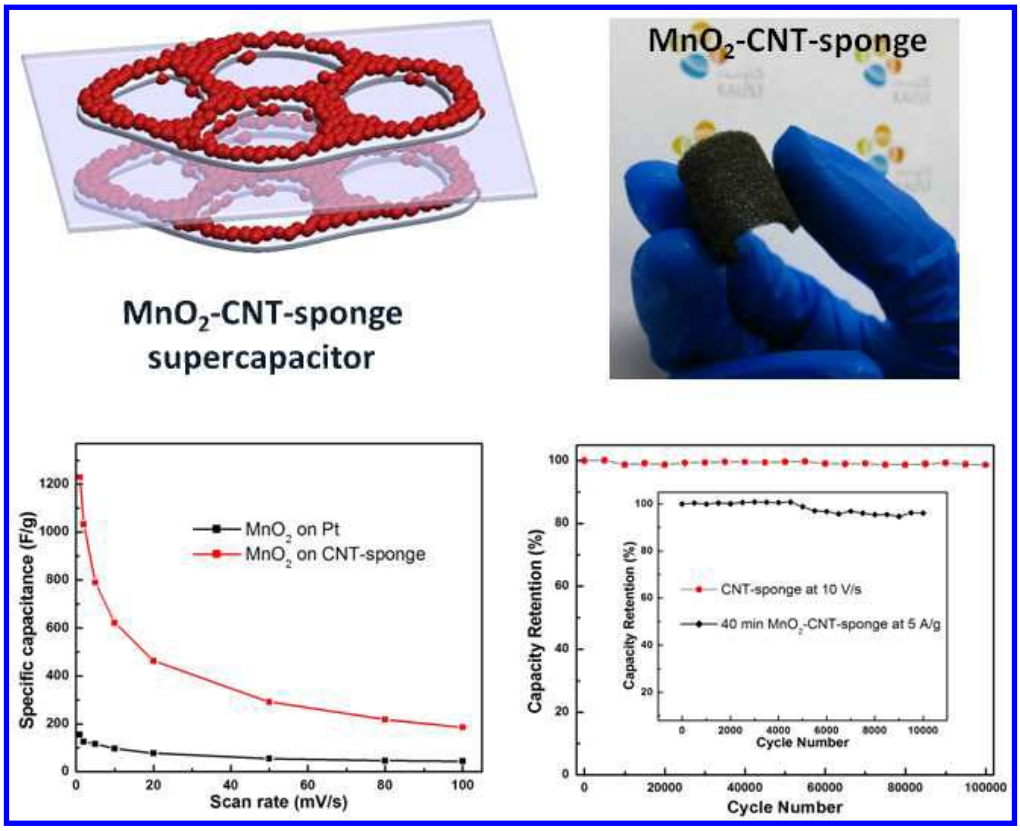

*Corresponding author: husam.alshareef@kaust.edu.sa

Phone: Office: +966-(0)2-808-4477 | Cell: +966-(0)5-44700037

ABSTRACT

A simple and scalable method has been developed to fabricate nanostructured MnO_2-CNT-sponge hybrid electrodes. A novel supercapacitor, henceforth referred to as "sponge supercapacitor", has been fabricated using these hybrid electrodes with remarkable performance. Ultrahigh specific capacitance (based on the mass of MnO_2) of 1,230 F/g was achieved, which is close to the theoretical value of MnO_2. Capacitors based on CNT-sponge substrates (without MnO_2) can be operated even under an extremely high scan rate of 200 V/s, and they exhibit outstanding cycle performance with only 2% degradation after 100,000 cycles under a scan rate of 10 V/s. The MnO_2-CNT-sponge supercapacitors show only 4% of degradation after 10,000 cycles at a charge-discharge specific current of 5 A/g. The specific power and energy of the MnO_2-CNT-sponge supercapacitors are high with values of 63 kW/kg and 61 Wh/kg, respectively. The attractive performances exhibited by these sponge supercapacitors make them promising candidates for future high performance energy storage systems.

KEYWORDS: sponge supercapacitor, energy storage, specific capacitance, specific power, MnO_2, carbon nanotubes.

Supercapacitors, also known as ultracapacitors, are promising energy storage devices that bridge the gap between batteries and conventional capacitors. Supercapacitors can provide higher energy density than conventional capacitors and much higher power density than batteries[1-4]. They exhibit a promising set of features such as high power density, fast rates of charge-discharge, reliable cycling life and safe operation[1-5]. Supercapacitors can be divided into two categories based on the underlying energy storage mechanism[1,2,5]. One is electrochemical double layer capacitor (EDLC), where electrical energy is stored by electrostatic accumulation of charges[1]. EDLC can provide ultrahigh power and excellent cycle life due to fast and non-degradation process between electrode active materials and electrolyte[2]. However, the energy stored in EDLCs is limited by the finite electrical charge separation at the interface of electrode materials and electrolyte and the availability of surface area[4]. Another type of supercapacitor is the so-called pseudocapacitor[1-3,5], in which electrical energy is mainly stored by fast and reversible redox reactions. Because of the Faradaic process underpinning the energy stored in a pseudocapacitor, it has increased energy density but at the cost of power density and cycle life compared to EDLCs. Hybrid supercapacitors, combine these two charge storage mechanisms (Faradaic and non-Faradaic), resulting in improved device characteristics[1,2,4,6-11]. Typically, carbon based materials are good electrodes for EDLCs[12-16], while transition metal oxides and electrically conducting polymers are good candidates for pseducapacitors[17-20]. Among the different EDLC electrode materials, carbon nanotubes (CNTs) attracted the most attention due to their good conductivity, mechanical flexibility, and stable electrochemical behavior[12,21-24]. In comparison, MnO_2 is the most thoroughly investigated transition metal oxide for pseudocapacitors due to its high theoretical specific capacitance (1370 F/g)[25], relatively low cost, and environmental friendliness[17,26]. However, the theoretical capacitance of MnO_2 has rarely been achieved in experiment[25], mainly due to its poor electrical conductivity (10^{-5} – 10^{-6} S/cm). In order to get high specific capacitance from MnO_2, many studies have been conducted, most of which are based on incorporating MnO_2 with conductive materials and forming hybrid electrode structures.[7,8,26-28] Several examples of

MnO_2 based hybrid electrodes have been recently demonstrated. Hou *et al.* synthesized a MnO_2/CNT/conducting polymer ternary electrodes with a specific capacitance of 427 F/g (based on three-electrode setup)[29]. Bao *et al.* demonstrated flexible supercapacitors using Zn_2SnO_4/MnO_2 core/shell nanocable coated on carbon microfiber with a specific capacitance of 642.4 F/g (based on three-electrode setup)[30]. Very recently, Lang *et al.* developed a supercapacitor based on nanoporous gold and MnO_2, with a high specific capacitance of 1,145 F/g (based on two-electrode setup), which is close to the theoretical value[31]. However, these fabrication processes are either too complicated or limited in scalability. Previously, we have exploited paper and textile as substrates to fabricate supercapacitors since they provide highly porous structure for the fast access of ions to electrolytes[32-35]. Different from the paper and textile in the previous work, here we exploited sponge as the substrate for supercapacitors.

Sponges, with a hierarchical macroporous nature, have been widely used in our daily life as cleaning tools and can be found everywhere. Sponges are made up of many small cellulose or polyester fibers, which make them highly porous and strong absorbing media with significant internal surface area. A commercial sponge has been employed into our work, which has a high water absorption capacity. A simple experiment showed that it can absorb 45 times more water than its own weight. This indicates the good accessibility and compatibility of sponge to water and aqueous solutions. Sponges offer novel exciting characteristics different from paper and textile: first, Sponge has much more uniform size of macropores. The pore size can be in the range of 100-500 μm. Second, the cellulose or polyester fibers are interconnect virtually free of junctions. Therefore, continuous coating of conducting nanomaterials is much easier since there are no junctions to cross.

We have designed and fabricated high performance supercapacitors using a simple and scalable method. The fabrication process consisted of four simple steps, as illustrated in Figure 1. A piece of commercially available sponge (pore sizes 100-500 μm) was cleaned by water and acetone for several times (Fig.1 (a)). After drying completely in a vacuum oven, the sponge was cut into small ribbons with thickness of 1 mm and area of 1×2 cm^2. The sponge ribbons were subsequently coated with CNTs using a simple "dipping

and drying" process in CNT ink suspension (Fig.1 (b)) (for details, see Supporting Information). The next step was to electrodeposit MnO_2 nanoparticles on the CNT-coated sponge by galvanostatic electrochemical deposition (Fig.1 (c)). A very small current density (500 $\mu A/cm^2$) was required to obtain the desired nanostructure of MnO_2. To study the dependence of supercapacitor performance on MnO_2 deposition time, we deposited MnO_2 on CNT-sponge for different times: ranging from 3 minutes to 40 minutes. The deposition area of each sample was 1×1 cm^2. In the last step (Fig.1 (d)), two identical MnO_2-CNT-sponges were sandwiched with a piece of polymer separator dipped in 1 M Na_2SO_4 electrolyte inserted in between, and sealed in a coin cell to complete the symmetrical two electrode assembly (for details, see Supporting Information).

The weight of a clean 1×2 cm^2 sponge was about 10 mg, which is much lighter than the rigid metal and other flexible substrates with the same area[36-38]. Due to the mechanical flexibility of CNTs and strong van der Waals interactions between the macroporous sponge cellulose and CNTs, the CNTs can be easily coated onto the skeleton of a sponge, rendering the insulating sponge highly conductive by a simple dipping and drying process.[33] The CNT-sponge has a sheet resistance of 1 Ohm/square, measured by four points probe technique. After conformal coating of CNTs onto the skeleton of the sponge, it still maintained hierarchical macroporous nature where its intricate assembly of pores remained open to allow the flow of electrolyte (Supporting Fig. 1S-a). The CNTs coated on the sponge have formed a thin layer of CNT network wrapped around the skeleton of sponge (Supporting Fig. 1S-b, c). The amount of CNTs coating on sponge can be readily controlled by the dipping time and ink concentration. In this work, we optimized the dipping time to maximize the amount of CNTs coated on the sponge without blocking its pores. Undercoating degrades the conductivity of the CNT-sponge electrode while overcoating closes the pores of the sponge and prevents the movement of the electrolyte ions. The mechanical resilience of the CNT-sponge skeleton was tested by folding, twisting, and stretching it repeatedly as shown in Supporting Fig. 4S-d, e, f. After all the mechanical tests, the CNT-sponge always reverted to its original shape without any permanent deformation.

SEM images of MnO_2-CNT-sponge showed clearly the three-dimensional (3D) hierarchical macroporous open-pore structure (Fig. 2a, Supporting Fig. 2S-a). Flower-like MnO_2 nanoparticles were uniformly deposited onto the conductive CNT-sponge skeleton, even at the edges (Fig. 2b, c, Supporting Fig. 2S-b, c). This further confirms that CNTs have been conformably coated on the sponge. Fig. 2a also shows an exciting point: the backbone of sponge is free of junctions and promotes the continuous coating of CNT to form excellent conducting pathways in the whole structure. After deposition of MnO_2, the highly porous nanostructure remained, which is good for the fast transportation of electrons and ions in the supercapacitor devices. The deposition mass of MnO_2 can be well controlled by adjusting the deposition time (Supporting Fig. 3S). We found that the surface of the CNT-sponge can be fully covered by MnO_2 after 10-minute electrodeposition (Supporting Fig. 3S-c). Increasing the deposition time will increase the mass loading and the thickness of MnO_2, as shown in the supporting information Fig. 3S. If the electrodeposition is run for one hour, a very thick film of MnO_2 with some cracks can be observed due to the large thickness (Supporting Fig. 3S-f). TEM images revealed that the nanostructure of MnO_2 is highly porous and includes many small nanoplates (Fig. 2d, Supporting Fig. 2S-d). The average pore size of the MnO_2 is around 3.2 nm and it has a BET specific surface area of 174 m^2/g (Supporting Fig. 4S). An HRTEM image together with selected area electron diffraction (SAED) pattern demonstrated that the deposited MnO_2 are polycrystalline (Fig. 2e and inset, Supporting Fig. 2S-e). We further confirmed that the polycrystalline MnO_2 nanoparticles belong to ε-MnO_2 by XRD (JCPDS 00-030-0820) (Fig. 2f). The flower-like MnO_2 nanoparticles on macroporous CNT-sponge essentially form a so-called double porous nanostructure[33]. This unique structure provides outstanding performance for the intercalation/de-intercalation of electrolyte cations into electrode materials, and we therefore expect a high performance supercapacitor.

The electrochemical performance of CNT-sponge substrate was tested using a two-electrode coin cell configuration. Two pieces of symmetrical CNT-sponge, one piece of separator and 1 M Na_2SO_4 have been used as electrodes, separator and electrolyte, respectively. All measurements have been conducted at

room temperature. As shown in Fig. 3a and b, the CNT-sponge devices (without MnO_2 deposition) can be operated over a wide range of scan rates: from 1 mV/s up to 200 V/s. The cyclic voltammograms retain the rectangular shape (which is characteristic of the ideal electrochemical double layer capacitive behavior) even at a high scan rate of 20 V/s. As expected, the currents increase with the applied scan rates, but surprisingly the CNT-sponge devices operates at the highest reported scan rate for aqueous electrolyte supercpacitors[7,25,28,35-38]. We can therefore conclude that ultrahigh power can be obtained from this kind of device[14]. Another good feature of the CNT-sponge device is its good electrochemical behavior even at an extremely high scan rate of 200 V/s, which is comparable to micro-supercapacitors built on rigid silicone substrates[14,16,39]. Furthermore, a linear dependence of the discharge current on the scan rate up to 8 V/s can be observed from Fig. 3c. The deviation of the linear dependence after 8 V/s is due to the diffusion limit of electrolyte ions to the electrode materials. The discharge currents are calculated from the discharge scan with an average over the whole voltage range at specific scan rates[14,39]. A mean areal capacitance of 0.36 mF/cm^2 can be obtained from the slope of Fig. 3c, which is comparable to the value of carbon materials based micro-supercapacitors[39]. A maximal value of 0.9 mF/cm^2 can also be obtained at a scan rate of 1 mV/s, but this value can be improved if more CNTs have been coated on the sponge. Fig. 3d illustrated the charge-discharge behavior of the CNT-sponge device. The figure shows ultrafast charge-discharge rate and linear dependence on voltage and time, with very small voltage drop at a specific current of 10 A/g. These results indicate that the CNT-sponge substrates used in the present work exhibit excellent supercapacitor performance. More importantly, these results coupled with other promising features of the CNT-sponge (such as ease of fabrication, low cost, light weight and flexibility) make it a highly promising energy storage substrate.

Fig. 4e shows the MnO_2-CNT-sponge electrodes prepared by electrochemical deposition of MnO_2 onto conductive CNT-sponge. The amount of MnO_2 was controlled by the deposition time. Here, we varied the deposition time from 3 minutes to 40 minutes. It was observed that as the deposition time increased, the mass loading of MnO_2 increased accordingly. This can be observed from the increased darkness of the

sponge as shown in Fig. 4b. The first ribbon on the left in Fig. 4b is a bare sponge, and the second one from the left is a CNT-sponge without MnO_2 on it. The remaining samples from left to right are MnO_2-CNT-sponge with deposition time from 3 minutes to 40 minutes. The color of the bottom part of the CNT-sponge becomes darker with increased electrodeposition time, which means more MnO_2 has been deposited on the sponge. This can be further confirmed by plotting the change of MnO_2 content and MnO_2 mass loading versus deposition time (Fig. 4a). As can be seen from Fig. 4a, the MnO_2 content (the weight percentage of MnO_2 in MnO_2-CNT composite) and its mass loading increased with the deposition time. Each data point in Fig. 4a is an average value of at least 10 samples. At low deposition time, e.g., 10 minute, the MnO_2 mass loading is around 0.1 mg/cm^2 and its content in the MnO_2-CNT composite is nearly 30% by weight. These values are higher than the values obtained from rigid metal substrates such as platinum at the same deposition time due to the large surface area of the sponge. When the electrodeposition time increased to 40 minutes, the mass loading of MnO_2 increased to 0.5 mg/cm^2, which is more than twice of CNT loading on the sponge, and the corresponding MnO_2 content in the MnO_2-CNT composite is as high as 67% by weight. For long deposition times, e.g. 20 hours, the mass loading of MnO_2 can go up to 12.8 mg/cm^2, which is twice of the weight than the CNT-sponge itself. To reveal the good adhesion between MnO_2 and CNT-sponge, a simple Scotch tape adhesion test was performed comparing the MnO_2-CNT-sponge and MnO_2-platinum electrodes. It can be seen clearly from Fig. 4c that superior adhesion performance is observed for the MnO_2-CNT-sponge: no peeling was observed in the case of MnO_2-CNT-sponge, while significant peeling was observed in the case of the rigid Pt foil (Fig. 4d). Another result that demonstrates the superior electrochemical performance of the MnO_2-CNT-sponge electrodes is comparing its cyclic voltammetry behavior to the flat MnO_2-Pt substrate. A three-electrode configuration has been setup to test the electrochemical performances by cyclic voltammogram (for details, see Supporting Information). At scan rate of 50 mV/s (Fig. 4f), the electrochemical performance of MnO_2-CNT-sponge outperforms that of MnO_2-Pt electrode in terms of wider voltage range and higher capacitance. At a five-minute electrodeposition of MnO_2, a very high specific capacitance of 1,230 F/g can be achieved from MnO_2-CNT-sponge electrode at scan rate of 1 mV/s. However, the value is just 155

F/g for MnO_2-Pt electrode under the same condition (Fig. 4g). This controlled experiment further confirms the outstanding electrochemical performance of MnO_2-CNT-sponge electrode.

To completely investigate the electrochemical performances of MnO_2-CNT-sponge supercapacitors, a typical two-electrode configuration has been employed in this work[40,41]. The MnO_2-CNT-sponge serves as electrode as well as current collector, and the integrated binder-free structure provides highly porous and conductive channels for the full access of electrolyte ions to the active electrode material in supercapacitors. As shown in Fig. 5a and b, the full cell has been studied by cyclic voltammograms over a wide range of scan rates: from 1 mV/s to 10 V/s. All samples behaved like ideal EDLCs at scan rates up to 1500 mV/s. Take the 5 minute MnO_2 deposition sample as an example. The CV shapes are almost rectangular at scan rates below 2 V/s and remain quasi-rectangular at scan rate up to 10 V/s, indicating the excellent charge storage characteristics and ultrafast response of the electrodes. The high scan rate of 10 V/s is two orders of magnitude higher than the rate used in most of the literature for the MnO_2/CNT composite electrodes with aqueous electrolyte[7,8,28-30]. The voltages versus time profiles were obtained by galvanostatic charge-discharge measurements (Fig. 5c). The device can be steadily operated over a wide range of applied specific current, from 1 A/g to 100 A/g. The internal resistances[41,42] (including the electrical resistances of electrodes, the ions diffusion resistances and the interfacial resistance between the electrode and electrolyte) derived from the voltage drop are consistent with the values calculated from impedance electrochemical spectroscopy (Supporting Fig. 5S). The cyclic voltammetry response of different samples under different deposition times have been demonstrated in Fig. 5d and e, at specific scan rate of 20 mV/s and 200 mV/s, respectively. The corresponding current increases with MnO_2 content on the electrodes for both scan rates, suggesting that more materials contributed to charge storage. When the scan rate changed from 20 mV/s to 200 mV/s, the CV shapes remained nearly rectangular, with only a few deviations for samples with high mass loading. This clearly shows the excellent electrochemical performance of the MnO_2-CNT-sponge supercapacitors. The specific capacitances with respect to the mass of MnO_2 have been derived from CVs and plotted in Fig. 5f, which are comparable with the values

calculated from galvanostatic charge-discharge curves. A specific capacitance of 1,000 F/g can be readily obtained based on the mass of MnO_2 at scan rate of 1 mV/s. The specific capacitances of MnO_2-CNT-sponge supercapacitor are one to two orders higher than that of CNT-sponge device, indicating the significant contribution from porous MnO_2, and these values are much higher than that from literature[29,30,35-38,43]. The specific capacitance decreases with the scan rates and MnO_2 deposition times, but remains constant at scan rates higher than 100 mV/s. The measured specific capacitance depends strongly on scan rate for low mass loading devices, but depends weakly on scan rate for high mass loading devices. For example, the specific capacitance decreased from 1,000 F/g at 1 mV/s to 581 F/g at 100 mV/s for the three-minute electrodeposition device. In comparison, it decreased from 444 F/g at 1 mV/s to 295 F/g at 100 mV/s for the ten-minute electrodeposition device. For higher mass loading devices, such as 30 minutes and 40 minutes MnO_2 depositions, negligible change in specific capacitance was observed, especially at high scan rates. This is mainly due to the limited conductivity of high mass loading samples and the limited utilization of MnO_2 at high scan rates. At low mass loading of MnO_2, the highly conductive double porous electrodes provide good opportunity for electron transportation and ions accessibility, maximizing the utilization of MnO_2 materials. At even lower deposition time, the theoretical specific capacitance can be practically achieved in this unique structure.

Looking into the charge storage mechanisms[2] of MnO_2-CNT-sponge supercapacitors, a possible electrochemical reaction can be proposed as the following:

$$MnO_2 + xH^+ + yNa^+ + (x+y)e^- \text{ <---> } MnOOH_xNa_y$$

The energy storage contributions come from both surface adsorption/desorption of electrolyte cations (Na^+) to the surface of CNTs and MnO_2, and the fast, reversible redox reactions by means of intercalation/extraction of protons into/out of MnO_2.[2,31] The conductive double porous structure facilitates the adsorption/desorption of Na^+ and the transportation of electrons and protons, allowing full access of the electrolyte to electrode materials and maximizing the utilization of MnO_2. Therefore, the cyclic

voltammograms exhibit the ideal rectangular shapes and a very high specific capacitance of 1,000 F/g can be readily obtained based on the mass of MnO_2.

Electrochemical impedance spectroscopy (EIS) and long time cycling stability are two important parameters to determine the performances of supercapacitors. Fig. 6a and inset show the Nyquist plots in the frequency range from 100 kHz to 0.01 Hz, which can be represented by the equivalent circuit and the corresponding model for ideal supercapacitors, as shown in Fig. 6b (ref. 1, 7, 30). In the equivalent circuit, a solution resistance (R_S) connects in series with a constant phase element (CPE), and the CPE connects in parallel with the charge transfer resistance (R_{CT}) and pseudo-capacitance (C_P). The solution resistance refers to the resistance from the electrolyte, the CPE accounts for the double-layer capacitance, and the charge transfer resistance (also called Faraday resistance) corresponds to the total resistance at the interface between the electrode and the electrolyte[44]. Experimental results show that R_S is insensitive to the surface condition of the electrode, and it is consistent with a value of around 1.5 Ω for all our devices. However, R_{CT} increases with the mass loading of MnO_2 on the surface of the CNT-sponge, from 4.5 Ω at 3-min MnO_2 electrodeposition to 28 Ω at 40-min deposition (Fig. 6a). Typically, the Nyquist plot can be divided by the so-called knee frequency into a high frequency semicircle and a low frequency vertical line[44], as schematically illustrated in Fig. 6b. The semi-circle intersection with the abscissa depends on the internal resistance and the vertical line implies good capacitive behaviors of supercapacitors. The internal resistances (including R_S, R_{CT} and other resistances) of all samples are summarized and plotted in Supporting Fig. 5S. These values are consistent with those derived from the voltage drop of charge-discharge curves. This result clearly indicates that the internal resistance increases with the MnO_2 deposition time due to increased mass loading of semiconducting MnO_2, making the MnO_2-CNT-sponge electrode less conductive. A long time charge-discharge cycling up to 100,000 cycles has been performed on CNT-sponge devices using a scan rate of 10 V/s. The results, shown in Fig. 6c, indicate that 98% of the initial capacitance is retained. In comparison, the cycling stability of MnO_2-CNT-sponge supercapacitors was also investigated up to 10,000 charge-discharge cycles using a specific current of 5

A/g. It is seen that 96% of the initial capacitance has been retained after 10,000 cycles (Fig. 6c inset) for the 40-minute MnO_2 deposition device. These results demonstrate good stability of both CNT-sponge and MnO_2-CNT-sponge supercapacitors. Fig. 6d shows a Ragone plot of MnO_2-CNT-sponge supercapacitors. The Ragone plot shows that the specific energy and specific power values of our sponge supercapacitors are higher than the ones reported in the literature[22,27,30,31,43,45,46], with maximum specific energy of 61 Wh/kg and specific power of 63 kW/kg. The CNT-sponge device showed ultrahigh specific power of 105 kW/kg, although the specific energy is low. All the specific energy and power values were calculated from the galvanostatic charge-discharge curves. These values demonstrate the outstanding capability of CNT-sponge and MnO_2-CNT-sponge supercapacitors as high power and high energy storage systems.

In summary, novel sponge supercapacitors have been fabricated using a simple method while providing remarkable performance. The macroporous nature of the sponge along with the porous nature of the electrodeposited MnO_2 nanoparticles provided a double porous electrode structure giving good conductivity and full accessibility of electrolyte to MnO_2, improving the performances of MnO_2-CNT-sponge supercapacitors dramatically. The MnO_2-CNT-sponge supercapacitor exhibits very high specific capacitance, ultra fast charge-discharge rate, excellent cycling stability as well as good energy and power density, making it one of the most promising electrodes for high performance large-scale energy storage systems.

Supporting Information.

Materials and Methods and additional supporting figures. This material is available free of charge via the Internet at http://pubs.acs.org

ACKNOWLEDGEMENT

The authors thank for the characterization analysis provided by KAUST Advanced Imaging and Characterization Laboratory and Analytic Core Laboratory. W.C. acknowledges support from KAUST discovery fellowship. H.A. acknowledges the support from KAUST baseline fund. Y.C. acknowledges support from the King Abdullah University of Science and Technology (KAUST) Investigator Award (No. KUS-l1-001-12) and the Precourt Institute for Energy at Stanford. X.X. acknowledges support from the Stanford Graduate Fellowship.

References

(1) Conway, B. E. *Electrochemical Supercapacitors: Scientific Fundamentals and Technological Applications*; Kluwer Academic/Plenum: New York, 1999.

(2) Simon, P.; Gogotsi, Y. *Nature Materials* **2008**, *7*, 845.

(3) Winter, M.; Brodd, R. J. *Chemical Reviews* **2005**, *105*, 1021.

(4) Zhang, L. L.; Zhao, X. S. *Chemical Society Reviews* **2009**, *38*, 2520.

(5) Arico, A. S.; Bruce, P.; Scrosati, B.; Tarascon, J. M.; Van Schalkwijk, W. *Nature Materials* **2005**, *4*, 366.

(6) Chen, Z.; Augustyn, V.; Wen, J.; Zhang, Y. W.; Shen, M. Q.; Dunn, B.; Lu, Y. F. *Advanced Materials* **2011**, *23*, 791.

(7) Liu, J. W.; Essner, J.; Li, J. *Chemistry of Materials* **2010**, *22*, 5022.

(8) Reddy, A. L. M.; Shaijumon, M. M.; Gowda, S. R.; Ajayan, P. M. *Journal of Physical Chemistry C* **2010**, *114*, 658.

(9) Mai, L.-Q.; Yang, F.; Zhao, Y.-L.; Xu, X.; Xu, L.; Luo, Y.-Z. *Nat Commun* **2011**, *2*, 381.

(10) Rakhi, R. B.; Cha, D.; Chen, W.; Alshareef, H. N. *The Journal of Physical Chemistry C* **2011**, *115*, 14392.

(11) Chen, S.; Zhu, J.; Wu, X.; Han, Q.; Wang, X. *ACS Nano* **2010**, *4*, 2822.

(12) Frackowiak, E.; Beguin, F. *Carbon* **2001**, *39*, 937.

(13) Chmiola, J.; Largeot, C.; Taberna, P. L.; Simon, P.; Gogotsi, Y. *Science* **2010**, *328*, 480.

(14) Pech, D.; Brunet, M.; Durou, H.; Huang, P. H.; Mochalin, V.; Gogotsi, Y.; Taberna, P. L.; Simon, P. *Nature Nanotechnology* **2010**, *5*, 651.

(15) Stoller, M. D.; Park, S. J.; Zhu, Y. W.; An, J. H.; Ruoff, R. S. *Nano Letters* **2008**, *8*, 3498.

(16) Gao, W.; Singh, N.; Song, L.; Liu, Z.; Reddy, A. L. M.; Ci, L.; Vajtai, R.; Zhang, Q.; Wei, B.; Ajayan, P. M. *Nat Nano* **2011**, *6*, 496.

(17) Lee, H. Y.; Goodenough, J. B. *Journal of Solid State Chemistry* **1999**, *144*, 220.

(18) Hu, C. C.; Tsou, T. W. *Electrochemistry Communications* **2002**, *4*, 105.

(19) Wang, Y. G.; Li, H. Q.; Xia, Y. Y. *Advanced Materials* **2006**, *18*, 2619.

(20) Rakhi, R. B.; Alshareef, H. N. *Journal of Power Sources* **2011**, *196*, 8858.

(21) Futaba, D. N.; Hata, K.; Yamada, T.; Hiraoka, T.; Hayamizu, Y.; Kakudate, Y.; Tanaike, O.; Hatori, H.; Yumura, M.; Iijima, S. *Nature Materials* **2006**, *5*, 987.

(22) An, K. H.; Kim, W. S.; Park, Y. S.; Moon, J. M.; Bae, D. J.; Lim, S. C.; Lee, Y. S.; Lee, Y. H. *Advanced Functional Materials* **2001**, *11*, 387.

(23) Pushparaj, V. L.; Shaijumon, M. M.; Kumar, A.; Murugesan, S.; Ci, L.; Vajtai, R.; Linhardt, R. J.; Nalamasu, O.; Ajayan, P. M. *Proceedings of the National Academy of Sciences of the United States of America* **2007**, *104*, 13574.

(24) Kaempgen, M.; Chan, C. K.; Ma, J.; Cui, Y.; Gruner, G. *Nano Letters* **2009**, *9*, 1872.

(25) Toupin, M.; Brousse, T.; Belanger, D. *Chemistry of Materials* **2004**, *16*, 3184.

(26) Wei, W. F.; Cui, X. W.; Chen, W. X.; Ivey, D. G. *Chemical Society Reviews* **2011**, *40*, 1697.

(27) Wu, Z. S.; Ren, W. C.; Wang, D. W.; Li, F.; Liu, B. L.; Cheng, H. M. *Acs Nano* **2010**, *4*, 5835.

(28) Lee, S. W.; Kim, J.; Chen, S.; Hammond, P. T.; Shao-Horn, Y. *Acs Nano* **2010**, *4*, 3889.

(29) Hou, Y.; Cheng, Y. W.; Hobson, T.; Liu, J. *Nano Letters* **2010**, *10*, 2727.

(30) Bao, L. H.; Zang, J. F.; Li, X. D. *Nano Letters* **2011**, *11*, 1215.

(31) Lang, X. Y.; Hirata, A.; Fujita, T.; Chen, M. W. *Nature Nanotechnology* **2011**, *6*, 232.

(32) Hu, L.; Choi, J. W.; Yang, Y.; Jeong, S.; La Mantia, F.; Cui, L.-F.; Cui, Y. *Proceedings of the National Academy of Sciences* **2009**, *106*, 21490.

(33) Hu, L.; Pasta, M.; Mantia, F. L.; Cui, L.; Jeong, S.; Deshazer, H. D.; Choi, J. W.; Han, S. M.; Cui, Y. *Nano Letters* **2010**, *10*, 708.

(34) Pasta, M.; La Mantia, F.; Hu, L.; Deshazer, H.; Cui, Y. *Nano Research* **2010**, *3*, 452.
(35) Yu, G.; Hu, L.; Vosgueritchian, M.; Wang, H.; Xie, X.; McDonough, J. R.; Cui, X.; Cui, Y.; Bao, Z. *Nano Letters* **2011**, *11*, 2905.
(36) Rajendra Prasad, K.; Miura, N. *Electrochemistry Communications* **2004**, *6*, 1004.
(37) Horng, Y.-Y.; Lu, Y.-C.; Hsu, Y.-K.; Chen, C.-C.; Chen, L.-C.; Chen, K.-H. *Journal of Power Sources* **2010**, *195*, 4418.
(38) Chou, S.-L.; Wang, J.-Z.; Chew, S.-Y.; Liu, H.-K.; Dou, S.-X. *Electrochemistry Communications* **2008**, *10*, 1724.
(39) Pech, D.; Brunet, M.; Taberna, P. L.; Simon, P.; Fabre, N.; Mesnilgrente, F.; Conedera, V.; Durou, H. *Journal of Power Sources* **2010**, *195*, 1266.
(40) Stoller, M. D.; Stoller, S. A.; Quarles, N.; Suk, J. W.; Murali, S.; Zhu, Y. W.; Zhu, X. J.; Ruoff, R. S. *Journal of Applied Electrochemistry* **2011**, *41*, 681.
(41) Stoller, M. D.; Ruoff, R. S. *Energy & Environmental Science* **2010**, *3*, 1294.
(42) Lei, Z. B.; Christov, N.; Zhao, X. S. *Energy & Environmental Science* **2011**, *4*, 1866.
(43) Yan, J. A.; Khoo, E.; Sumboja, A.; Lee, P. S. *Acs Nano* **2010**, *4*, 4247.
(44) Li, X.; Rong, J.; Wei, B. *ACS Nano* **2010**, *4*, 6039.
(45) Cottineau, T.; Toupin, M.; Delahaye, T.; Brousse, T.; Belanger, D. *Applied Physics a-Materials Science & Processing* **2006**, *82*, 599.
(46) Zhou, C. F.; Kumar, S.; Doyle, C. D.; Tour, J. M. *Chemistry of Materials* **2005**, *17*, 1997.

Figures

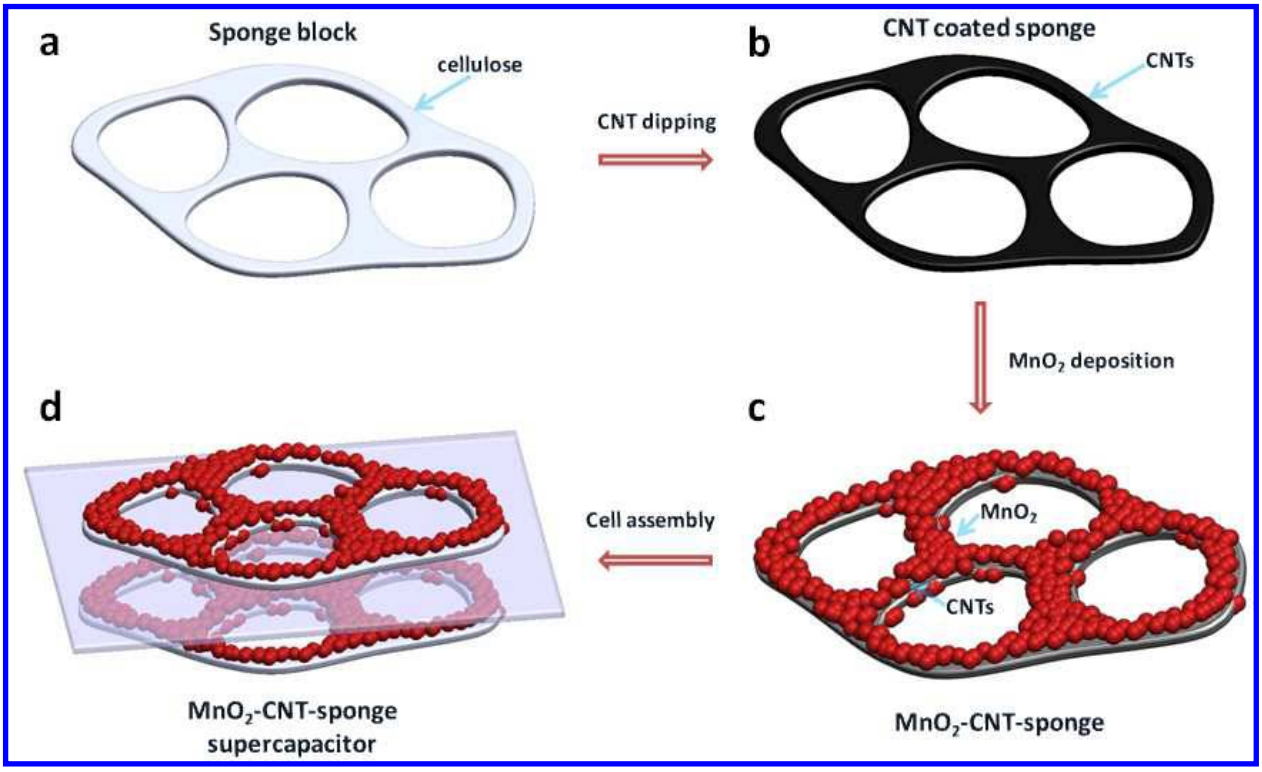

Figure 1 Fabrication process of MnO_2-CNT-sponge supercapacitors. (a) A piece of sponge is cleaned and cut into small ribbons; (b) CNTs are coated onto the skeleton of the sponge by a "dipping and drying" method; (c) Nanostructured MnO_2 is electrodeposited onto the conductive CNT-sponge skeleton; (d) Two pieces of MnO_2-CNT-sponge electrodes were assembled into coin cell to form a MnO_2-CNT-sponge supercapacitor.

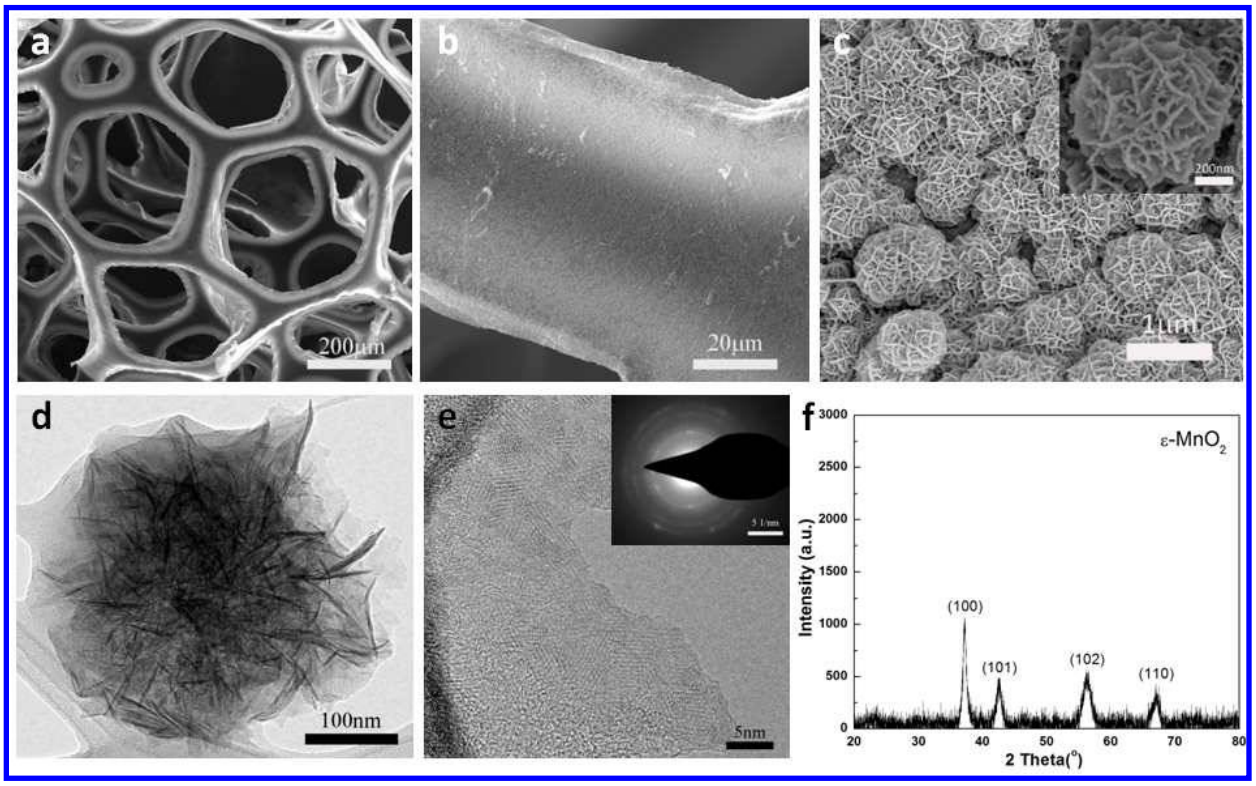

Figure 2 Characterizations of MnO_2-CNT-sponge electrodes. a, An overall view of 3D macroporous hierarchical MnO_2-CNT-sponge electrode. b, MnO_2 uniformly deposited on the skeleton of CNT-sponge. c, High magnification of porous MnO_2 nanoparticles on CNT-sponge, inset shows morphology of an individual MnO_2 flower-like particle. d, A TEM image of MnO_2 shows highly porous structure. e, HRTEM image and the inset SAED pattern of porous MnO_2 showing the polycrystalline nature of MnO_2. f, XRD of the as-synthesized structure showing the ε-MnO_2 phase.

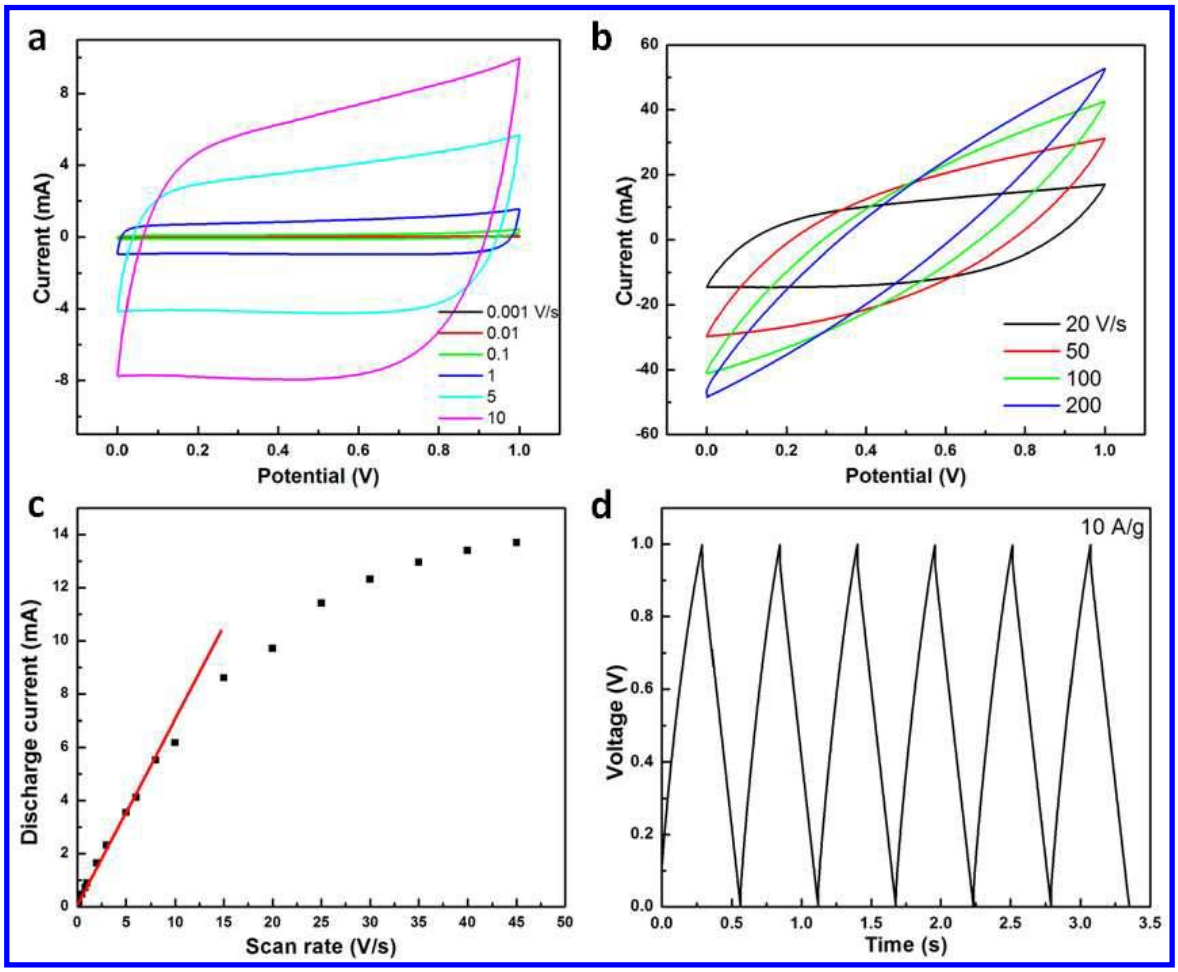

Figure 3 Electrochemical behaviors of CNT-sponge substrates. a and b, Cyclic voltammetry scan from 1 mV/s to 10 V/s, and from 20 V/s to 200 V/s, respectively. c, Discharge currents as a function of scan rates (linear relation is obtained up to scan rate of 8 V/s). d, Galvanostatic charge-discharge curves at a specific current of 10 A/g.

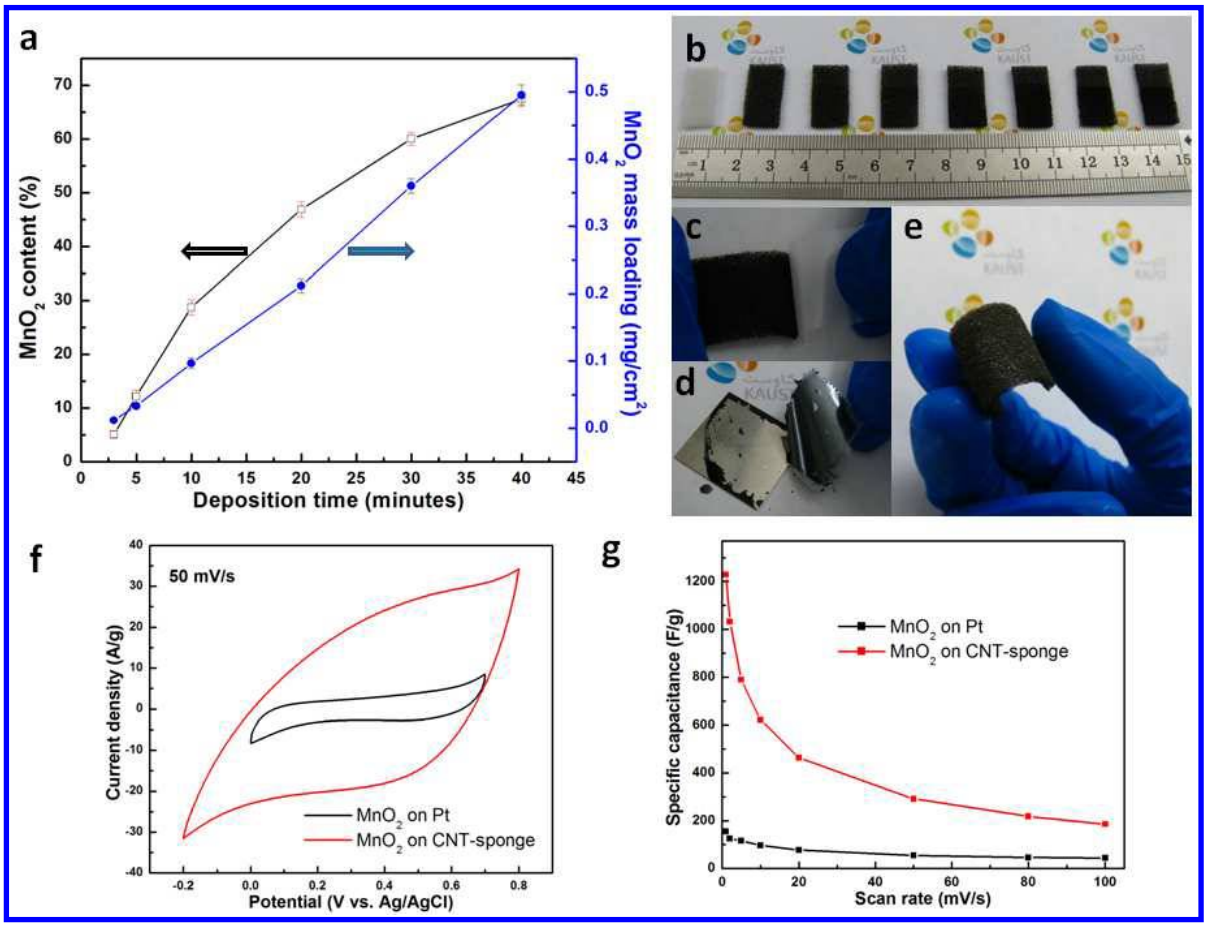

Figure 4 MnO_2-CNT-sponge supercapacitor electrodes. a, MnO_2 content and mass loading vs. elctrodeposition time from 3 minutes to 40 minutes. b, Photograph of MnO_2-CNT-sponge electrodes array, the samples from left to right are corresponding to: bare sponge, CNT-sponge, MnO_2 deposition on CNT-sponge for 3, 5, 10, 20, 30 and 40 minutes. c and d, Photograph of Scotch tape tests of MnO_2-CNT-sponge and MnO_2-Pt electrode, respectively. e, Photograph of a MnO_2-CNT-sponge electrode. f, CV of MnO_2 on Pt vs. MnO_2 on CNT-sponge at 50 mV/s. g, Specific capacitance comparison between MnO_2-Pt and MnO_2-CNT-sponge.

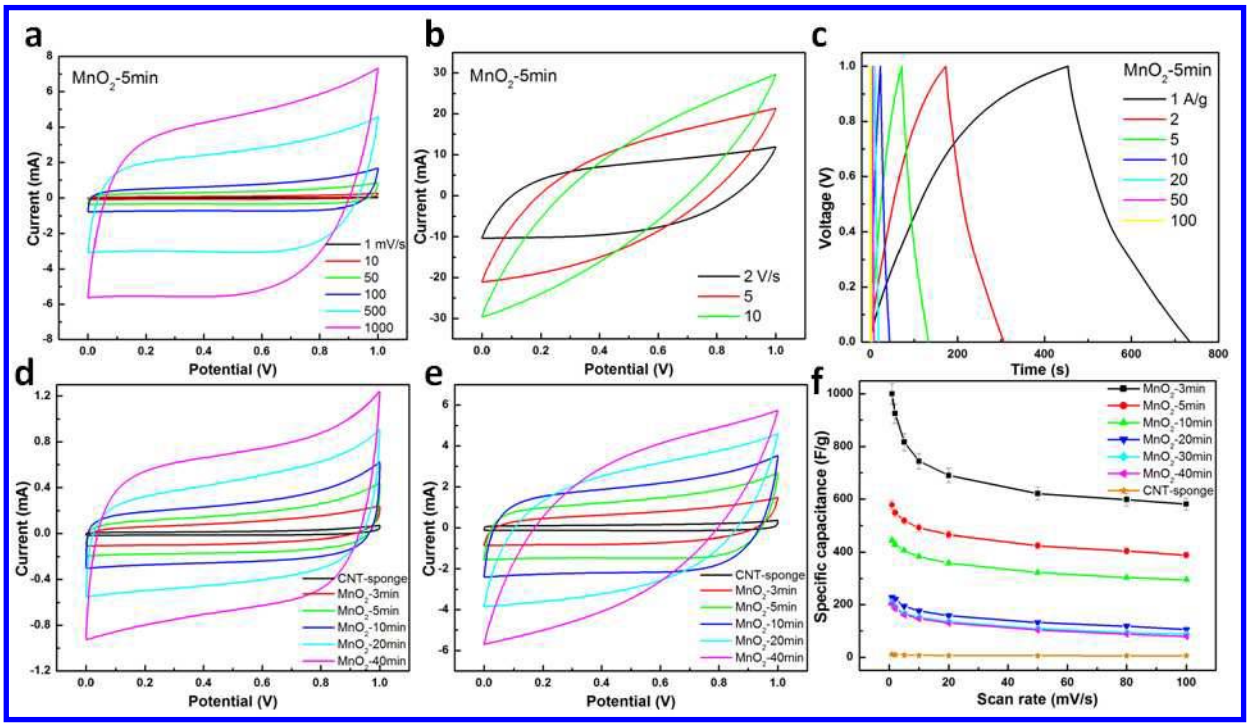

Figure 5 Electrochemical performances of MnO_2-CNT-sponge supercapacitors. a and b, Cyclic voltammograms of a 5-minute MnO_2 deposition device at low and high scan rates, respectively. c, Galvanostatic charge-discharge of a 5-minute MnO_2 deposition device under different current densities. d and e, Cyclic voltammograms of device with different MnO_2 deposition times at scan rate of 20 mV/s and 200 mV/s, respectively. f, Specific capacitance versus scan rate for devices with different MnO_2 deposition time, ranging from 0 minute to 40 minutes. All data are taken in a 1 M Na_2SO_4 full cell at room temperature.

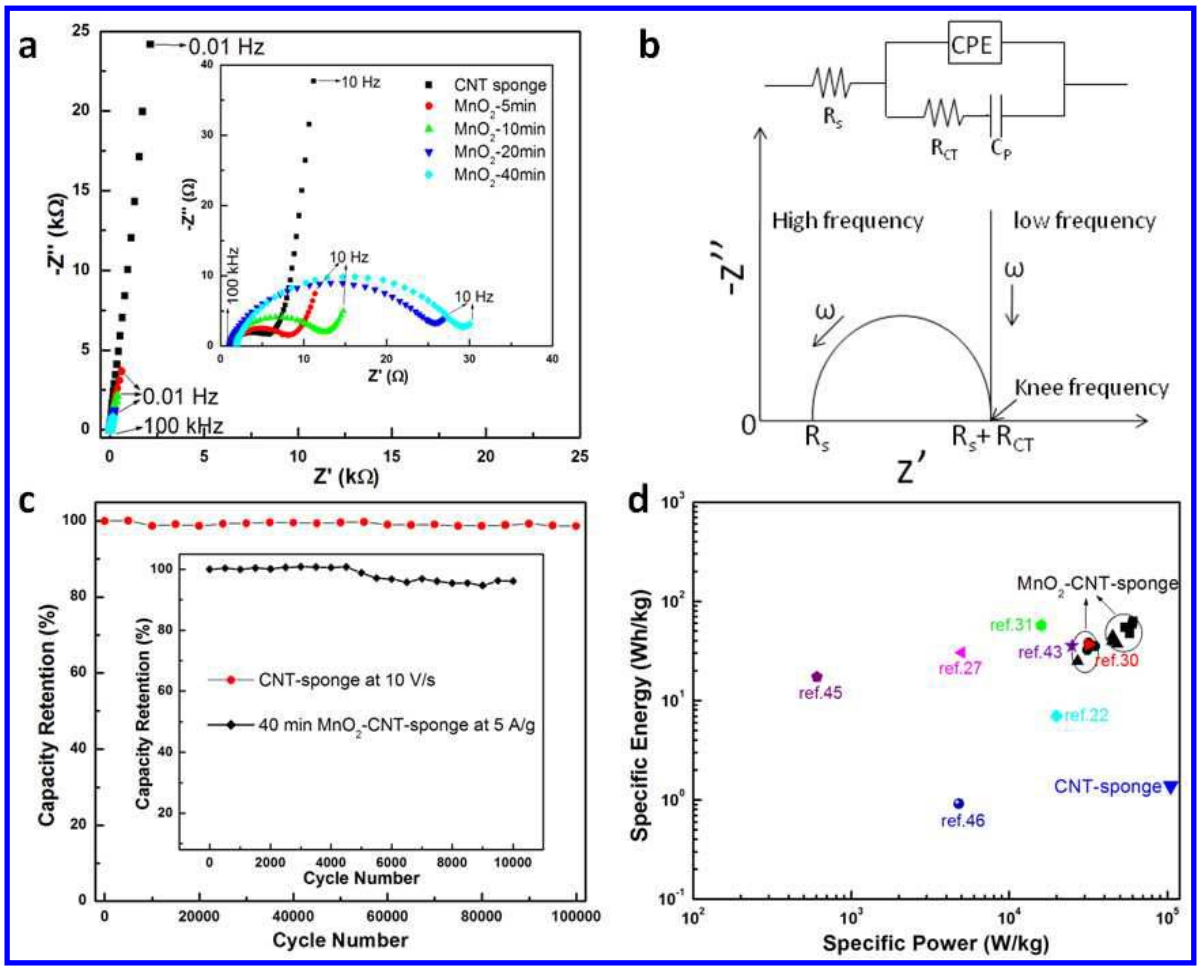

Figure 6 Nyquist plot, equivalent circuit model, long time cycling and Ragone plot of MnO_2-CNT-sponge supercapacitors. a, Nyquist plot of supercapacitor devices with different MnO_2 deposition times, ranging from 0 to 40 minutes. b, Equivalent circuit model of the device c, Capacity retention versus cycle number for CNT-sponge device up to 100,000 cycles at a high scan rate of 10 V/s and 40 minutes MnO_2-CNT-sponge supercapacitors under 10,000 cycles at a specific current of 5 A/g, respectively. d, Ragone plot of MnO_2-CNT-sponge supercapacitors and CNT-sponge devices compared with other literature.